



**HAL**  
open science

## **JWST Discovery of Dust Reservoirs in Nearby Type IIP Supernovae 2004et and 2017eaw**

Melissa Shahbandeh, Arkaprabha Sarangi, Tea Temim, Tamás Szalai, Ori D. Fox, Samaporn Tinyanont, Eli Dwek, Luc Dessart, Alexei V. Filippenko, Thomas G. Brink, et al.

► **To cite this version:**

Melissa Shahbandeh, Arkaprabha Sarangi, Tea Temim, Tamás Szalai, Ori D. Fox, et al.. JWST Discovery of Dust Reservoirs in Nearby Type IIP Supernovae 2004et and 2017eaw. *Monthly Notices of the Royal Astronomical Society*, 2023, 523 (4), pp.6048-6060. 10.1093/mnras/stad1681. hal-03982542

**HAL Id: hal-03982542**



**<https://hal.science/hal-03982542>**

Submitted on 3 Jan 2024

**HAL** is a multi-disciplinary open access archive for the deposit and dissemination of scientific research documents, whether they are published or not. The documents may come from teaching and research institutions in France or abroad, or from public or private research centers.

L'archive ouverte pluridisciplinaire **HAL**, est destinée au dépôt et à la diffusion de documents scientifiques de niveau recherche, publiés ou non, émanant des établissements d'enseignement et de recherche français ou étrangers, des laboratoires publics ou privés.

# JWST observations of dust reservoirs in type IIP supernovae 2004et and 2017eaw

Melissa Shahbandeh <sup>1,2★</sup>, Arkaprabha Sarangi <sup>3</sup>, Tea Temim,<sup>4</sup> Tamás Szalai <sup>5,6</sup>, Ori D. Fox <sup>2★</sup>, Samaporn Tinyanont <sup>7</sup>, Eli Dwek,<sup>8</sup> Luc Dessart,<sup>9</sup> Alexei V. Filippenko,<sup>10</sup> Thomas G. Brink,<sup>10</sup> Ryan J. Foley,<sup>7</sup> Jacob Jencson,<sup>1</sup> Justin Pierel,<sup>2</sup> Szanna Zsíros,<sup>5</sup> Armin Rest,<sup>1,2</sup> WeiKang Zheng,<sup>10</sup> Jennifer Andrews,<sup>11</sup> Geoffrey C. Clayton,<sup>12</sup> Kishalay De,<sup>13</sup> Michael Engesser,<sup>2</sup> Suvi Gezari,<sup>2</sup> Sebastian Gomez,<sup>2</sup> Shireen Gonzaga,<sup>2</sup> Joel Johansson,<sup>14</sup> Mansi Kasliwal,<sup>15</sup> Ryan Lau,<sup>16</sup> Ilse De Looze,<sup>17</sup> Anthony Marston <sup>18</sup>, Dan Milisavljevic <sup>19,20</sup>, Richard O’Steen <sup>2</sup>, Matthew Siebert,<sup>2</sup> Michael Skrutskie,<sup>21</sup> Nathan Smith <sup>22</sup>, Lou Strolger,<sup>2</sup> Schuyler D. Van Dyk <sup>23</sup>, Qinan Wang <sup>1</sup>, Brian Williams,<sup>8</sup> Robert Williams,<sup>2</sup> Lin Xiao<sup>24,25</sup> and Yi Yang <sup>10</sup>

*Affiliations are listed at the end of the paper*

Accepted 2023 May 12. Received 2023 May 12; in original form 2023 February 1

## ABSTRACT

Supernova (SN) explosions have been sought for decades as a possible source of dust in the Universe, providing the seeds of galaxies, stars, and planetary systems. SN 1987A offers one of the most promising examples of significant SN dust formation, but until the *James Webb Space Telescope (JWST)*, instruments have traditionally lacked the sensitivity at both late times ( $>1$  yr post-explosion) and longer wavelengths (i.e.  $>10\ \mu\text{m}$ ) to detect analogous dust reservoirs. Here we present *JWST*/MIRI observations of two historic Type IIP SNe, 2004et and SN 2017eaw, at nearly 18 and 5 yr post-explosion, respectively. We fit the spectral energy distributions as functions of dust mass and temperature, from which we are able to constrain the dust geometry, origin, and heating mechanism. We place a 90 per cent confidence lower limit on the dust masses for SNe 2004et and 2017eaw of  $>0.014$  and  $>4 \times 10^{-4} M_{\odot}$ , respectively. More dust may exist at even colder temperatures or may be obscured by high optical depths. We conclude dust formation in the ejecta to be the most plausible and consistent scenario. The observed dust is radiatively heated to  $\sim 100\text{--}150$  K by ongoing shock interaction with the circumstellar medium. Regardless of the best fit or heating mechanism adopted, the inferred dust mass for SN 2004et is the second highest (next to SN 1987A) mid-infrared inferred dust mass in extragalactic SNe thus far, promoting the prospect of SNe as potential significant sources of dust in the Universe.

**Key words:** supernovae: general – supernovae: individual: SN 2004et, SN 2017eaw – infrared: general – transients: supernovae.

## 1 INTRODUCTION

The source of the large amounts of dust observed in high-redshift galaxies remains uncertain (Maiolino et al. 2004). For over 50 yr, core-collapse supernovae (CCSNe) have been considered as possible sources of dust (Cernuschi & Codina 1967; Hoyle & Wickramasinghe 1970). Type II-P supernovae (SNe IIP), in particular, are likely candidates since they account for  $\sim 70$  per cent of all SNe II, and are plentiful enough that they could account for the observed dust at high redshifts (e.g. see Schneider, Ferrara & Salvaterra 2004; Dwek, Galliano & Jones 2007; Nozawa et al. 2008; Gall, Hjorth & Andersen 2011; and references therein). Models of expanding SN IIP ejecta succeed in condensing out sufficient quantities ( $0.1\text{--}1 M_{\odot}$ ; Todini & Ferrara 2001; Nozawa et al. 2003; Cherchneff & Dwek

2009; Sarangi & Cherchneff 2015; Sarangi, Matsuura & Micelotta 2018; Sluder, Milosavljević & Montgomery 2018).

A number of SNe of different subclasses were observed by the *Spitzer Space Telescope* (hereafter *Spitzer*), but measured dust masses were often too small to explain the amount of dust at high redshifts. Only a handful of nearby SNe II, let alone SNe IIP, have shown direct observational evidence for dust condensation, and these examples all yielded 2–3 orders of magnitude ( $<10^{-2} M_{\odot}$ ) less dust than predicted by the above models (e.g. Gerardy et al. 2002; Pozzo et al. 2004; Sugerman et al. 2006; Meikle et al. 2007, 2011; Andrews et al. 2010, 2011; Fabbri et al. 2011; Szalai et al. 2011). Renewed interest in SN dust began with several important advances: (i) the far-infrared/sub-mm/mm detection of a large amount of cold dust in SN 1987A (Matsuura et al. 2011, 2015; Indebetouw et al. 2014; Wesson et al. 2015), (ii) the detection of large quantities of dust in some Galactic SNRs (e.g. Owen & Barlow 2015; De Looze et al. 2017; Temim et al. 2017; Priestley et al. 2020), (iii) large dust masses ( $>10^{-2} M_{\odot}$ ) inferred from optical line profile asymmetries (Bevan &

\* E-mail: [melissa.shahbandeh@gmail.com](mailto:melissa.shahbandeh@gmail.com) (MS); [ofox@stsci.edu](mailto:ofox@stsci.edu) (ODF)

Barlow 2016; Bevan, Barlow & Milisavljevic 2017; Bevan et al. 2019), and (iii) the identification of isotopic anomalies in meteorites (e.g. Clayton & Nittler 2004).

Despite these promising discoveries, large dust reservoirs have not yet been directly observed at mid-infrared (mid-IR) wavelengths in extragalactic SNe, which could be due to a number of reasons. New dust condenses at high temperatures, but its temperature decreases rapidly with the expansion of the ejecta and the decay of internal radioactive heating sources. Consequently, the reservoirs of warm and cold (i.e. not hot) dust may only become detectable at longer wavelengths (Wesson et al. 2015). *Spitzer* was limited in its sensitivity at these wavelengths during the Cold Mission, which ended in 2008. After that point, *Spitzer* had access to only 3.6 and 4.5  $\mu\text{m}$  imaging. Furthermore, the timeline of dust growth is quite uncertain. Gall et al. (2014) suggest that accelerated dust growth does not begin until  $>5$  yr after explosion. However, Dwek, Sarangi & Arendt (2019) argue that the dust mostly forms at earlier epochs ( $<2$  yr) but is largely obscured due to optical-depth effects until the ejecta expand sufficiently and become optically thin at later epochs. The *Spitzer* observations could probe only the warmer dust components ( $>500$  K) and/or earlier epochs ( $<5$  yr). For the first time, *JWST*'s Mid-Infrared Instrument (MIRI) offers the possibility to probe cooler dust growth in extragalactic SNe (e.g. Hosseinzadeh et al. 2022).

Here we present MIRI imaging observations of two SNe IIP, 2004et and 2017eaw, as part of *JWST* GO-2666 (PI O Fox). SN 2004et was discovered by S Moretti on 2004 September 27 UT (Zwitter, Munari & Moretti 2004) and SN 2017eaw was discovered on 2017 May 14.24 UT (Dong & Stanek 2017; Wiggins 2017). Both SNe are located in the nearby, face-on spiral galaxy NGC 6946, which has produced around a dozen known SNe and other luminous transients (including SNe IIP 1948B, 2002hh, the Type IIL SN 1980K, and the ‘SN impostor’ SN 2008S). The two SNe are positioned close to the outer boundary of the spiral arms with high metallicity in NGC 6946. Both photometric and spectral evolution of SNe 2004et and SN 2017eaw seem to be quite similar and correspond well to those of ‘normal’ SN IIP explosions. The *Spitzer* photometry of both SNe show a similar decline rate to that of a typical SN IIP (Tinyanont et al. 2019). For both SNe, the evolution of the emission-line profiles and the decline rate of their light curves suggest dust formation at around 300 d (Sahu et al. 2006; Szalai et al. 2019; Tinyanont et al. 2019). However, SN 2004et was a bit more luminous than SN 2017eaw (they reached a peak  $V$  magnitude of 12.6 and 12.8, respectively; see e.g. Sahu et al. 2006; Maguire et al. 2010; Tsvetkov et al. 2018; Buta & Keel 2019; Szalai et al. 2019; Van Dyk et al. 2019). SN 2004et also shows a rebrightening at around 1000 d, which could be due to either ejecta–circumstellar material (ejecta–CSM) interaction, or to a thermal echo (Kotak et al. 2009). At similar epochs, only NEOWISE photometry was available for SN 2017eaw; if any similar late-time rebrightening occurred, it would probably not have been detectable due to the sensitivity and sampling of NEOWISE data.

The search for potential progenitors of both SNe in archival imaging started right after their discoveries. For SN 2004et, Li et al. (2005) identified a yellow supergiant on *Canada–France–Hawaii Telescope* images. Later, Crockett et al. (2011) showed that this source was still visible years after explosion and – based on high-resolution post-explosion images obtained by William Herschel Telescope, *Hubble Space Telescope* (*HST*), and the Gemini telescope – the progenitor is rather a late-K to late-M supergiant of  $M_{\text{prog}} = 8_{-1}^{+5} M_{\odot}$ . Nevertheless, hydrodynamic and semi-analytical modeling of optical light curves lead to an ejecta mass of  $\sim 11$ – $23 M_{\odot}$  (Utrobin &

Chugai 2009; Nagy et al. 2014; Morozova, Piro & Valenti 2018; Martinez & Bersten 2019; Ricks & Dwarkadas 2019), implying a much larger progenitor mass. Using non-local thermodynamic equilibrium time-dependent radiative transfer calculations, a good match to the multiband light curve and spectral evolution was obtained by Hillier & Dessart (2019) for a solar-metallicity  $15 M_{\odot}$  progenitor exploding as a red-supergiant star with a final mass of  $13.8 M_{\odot}$ , producing ejecta with a mass of  $12.1 M_{\odot}$  and  $1.2 \times 10^{51}$  erg kinetic energy. Using the method of late-time spectral modeling, Jerkstrand et al. (2012) determined a value of  $M_{\text{prog}} \approx 15 M_{\odot}$  for SN 2004et, only marginally above the inference of Hillier & Dessart (2019).

In the case of SN 2017eaw, archival *HST* and *Large Binocular Telescope* images enabled the identification of the progenitor as a red supergiant (RSG) star with an estimated initial mass of  $M_{\text{prog}} \approx 11$ – $17 M_{\odot}$  (van Dyk et al. 2017; Johnson, Kochanek & Adams 2018; Kilpatrick & Foley 2018; Rui et al. 2019). Modeling of optical light curves and nebular spectra (Szalai et al. 2019), as well as of near-infrared (NIR) spectra (Rho et al. 2018), consistently give  $M_{\text{prog}} \approx 15 M_{\odot}$ . Note that Williams et al. (2018) give a much lower value for the progenitor mass ( $8.8_{-0.2}^{+2.0} M_{\odot}$ ) of SN 2017eaw from modeling the local stellar population.

Both SNe also show evidence for early dust formation in their ejecta. For SN 2004et, Kotak et al. (2009) and Fabbri et al. (2011) present one of the most detailed mid-IR *Spitzer* data sets of an SN including four-channel IRAC (3.6–8.0  $\mu\text{m}$ ), MIPS (24.0  $\mu\text{m}$ ), and IRS measurements. For SN 2017eaw, near-IR spectra and photometry, accompanied by 3.6- and 4.5  $\mu\text{m}$  *Spitzer* photometry, were used for giving estimates of the properties of early-time dust (Rho et al. 2018; Tinyanont et al. 2019, see details later).

SNe 2004et and 2017eaw belong to the small group of just several SNe IIP [i.e. 2004dj, 2006od, 2011ja, and 2013ej; Tinyanont et al. (2019), and those within] showing signs of CSM interaction. Early-time radio (SN 2004et: Beswick et al. 2004; Stockdale et al. 2004; Martí-Vidal et al. 2007; Misra et al. 2007; SN 2017eaw: Argo et al. 2017; Nayana & Chandra 2017) and X-ray (SN 2004et: Misra et al. 2007; Rho et al. 2007; SN 2017eaw: Grefenstette, Harrison & Brightman 2017; Kong & Li 2017) detections, giving the highest fluxes among SNe II-P, have already implied the presence of (moderate) CSM in the vicinity of both SNe (Chevalier, Fransson & Nymark 2006; Szalai et al. 2019). In the case of SN 2017eaw, an early bump peaking at  $\sim 6$ – $7$  d after explosion in all optical bands also supports this picture (Szalai et al. 2019). Moreover, based on archival *Spitzer* images, Kilpatrick & Foley (2018) showed that the progenitor of SN 2017eaw was surrounded by a dusty shell at  $\sim 4000 R_{\odot}$ . Final evidence for the presence of CSM was the detection of strong  $H\alpha$  emission with a box-like line profile in both SNe  $\sim 2.5$  yr after explosion (Kotak et al. 2009; Maguire et al. 2010; Weil et al. 2020) and very late-time optical detections (Rizzo Smith, Kochanek & Neustadt 2022); these findings also strengthen the picture on the similarity of the two exploded stars and of their environments.

Combined light-curve analysis of SNe 2004et and 2017eaw also enabled an improved estimate of the distance of the host galaxy NGC 6946. While previous work gave values of  $D \approx 5.5$ – $6.1$  Mpc (Karachentsev, Sharina & Huchtmeier 2000; Herrmann et al. 2008; Bose & Kumar 2014), Szalai et al. (2019) showed that the distance of NGC 6946 is probably larger by  $\sim 30$  percent, in agreement with the values given by the tip-of-the-red-giant-branch (TRGB) method (Tikhonov 2014; Anand, Rizzi & Tully 2018; Eldridge & Xiao 2019). In this paper, we

use the latest TRGB distance<sup>1</sup> of  $D = 7.12$  Mpc ( $\mu = 29.26$  mag).

The results presented throughout this paper have not been corrected for extinction. The Galactic foreground extinction to NGC 6946 is known to be large,  $A_V \sim 1$  mag generally (Jerkstrand et al. 2012; Van Dyk et al. 2019), given its relatively low Galactic latitude, irrespective of internal host extinction. However, we found that the overall impact, even of these large values, on the results are relatively small. Although the specific extinction values for the MIRI filters are not well-defined, we estimate values from Xue et al. (2016; their fig. 20), where we assume that  $A_{K_S}/A_V = 0.11$  (Rieke & Lebofsky 1985).

In Section 2 of this paper, we present our observations and reductions. Section 3 describes the dust formation physical scenarios and our dust models. We interpret the results in Section 4 and discuss the dust masses relative to those of other historic SNe. A summary of our results and the conclusions are given in Section 5.

## 2 OBSERVATIONS AND DATA REDUCTION

### 2.1 JWST/MIRI imaging

As part of the Cycle 1 General Observers (GO) 2666 programme (PI O Fox; DOI: 10.17909/8kkm-fr55; <http://dx.doi.org/10.17909/8kkm-fr55>), we obtained images of SNe 2004et and 2017eaw with the JWST Mid-Infrared Instrument (MIRI; Bouchet et al. 2015; Ressler et al. 2015; Rieke et al. 2015; Rieke & Wright 2022) on 2022 September 20 (6567 d post-explosion) and 2022 September 21 (1954 d post-explosion), respectively (see Fig. 1). The observations were acquired in the F560W, F1000W, F1130W, F1280W, F1500W, F1800W, F2100W, and F2550W filter bands, using the FASTR1 readout pattern in the FULL array mode and a four-point extended source dither pattern. The data were processed with the JWST Calibration Pipeline version 1.7.2, using the Calibration Reference Data System version 11.16.9.

A ‘background image’ was constructed for each filter by taking a sigma-clipped average of the individual dithers in detector coordinates, and this background was then subtracted from the calibrated (level two) individual dither images in the corresponding filter. The background-subtracted level-2 images were then combined into a single calibrated image for each filter (Bright & JWST/MIRI Team 2016; Greenfield & Miller 2016; Bushouse et al. 2022). To measure the brightness of both SNe, we performed point spread function (PSF) photometry on background-subtracted level-2 data products using WebbPSF (Perrin et al. 2014). In order to calibrate the flux, we applied flux offsets by measuring the PSF of all the stars in the field and comparing them to the corresponding catalogs created by the pipeline. The fluxes of all four dithers of each filter were then averaged. Table 1 summarizes the PSF photometry for both SNe in terms of both flux and AB magnitude (Oke & Gunn 1983).

### 2.2 HST archival photometry

For part of this analysis (Section 4.2 below), we obtained HST images for the two SNe from the *Mikulski Archive for Space Telescopes* (MAST). Although all the data were previously published in separate papers, we reanalyse the data here to provide single, consistent set of photometry reduced with the latest version of the HST pipeline. We downloaded drizzled images from MAST, so they have been

processed through the standard pipeline at the Space Telescope Science Institute (STScI). Drizzled images are a combination of individual bias-subtracted, dark-subtracted, flat-fielded exposures that are then corrected for geometric distortion. We used the JWST-HST Alignment Tool (JHAT)<sup>2</sup> which applies a relative astrometric correction to each image by iteratively matching sources between observations, to ensure precise alignment between the HST and JWST data.

With all images aligned, the total SN flux was measured inside a circular aperture placed in each HST observation at the JWST SN location using the PYTHON package PHOTUTILS. The aperture radius was set to 3 pixels, or  $\sim 1.5$ –2 times the full width at half-maximum intensity for HST ACS and WFC3, owing to a nearby star contaminating the flux at larger radii. We subtract the local background flux from the aperture flux with the  $\sigma$ -clipped (using  $3\sigma$ ) median value in a circular annulus centred at the SN location, using an inner radius of 5 pixels and an outer radius of 7 pixels. This is sufficiently large that  $> 99.9$  per cent of the SN flux should be within the annulus inner radius, but small enough to ensure the neighboring star contamination and background light are removed. Finally, the measured flux for each image was corrected using aperture corrections from the public ACS/WFC3 encircled energy tables,<sup>3,4</sup> and converted to AB magnitudes using the time-dependent inverse sensitivity and filter pivot wavelengths provided with each data file.

### 2.3 Spitzer archival photometry

SN 2004et was observed with the *Spitzer* InfraRed Array Camera (IRAC; Fazio et al. 2004) from 2004 to 2019. Data during the Cold Mission of *Spitzer*, prior to 2009 May, were obtained in all four IRAC channels, while later data during the Warm Mission were obtained in the 3.6- and 4.5- $\mu\text{m}$  channels. Photometry up to 1803 d post-explosion was published by Kotak et al. (2009) and Fabbri et al. (2011). The bulk of the late-time data after 2014 was obtained as part of the SPITZER InfraRed Intensive Transients Survey (SPIRITS; Tinyanont et al. 2016; Kasliwal et al. 2017; Jencson et al. 2019).

To perform new photometry on the 3.6- and 4.5- $\mu\text{m}$  IRAC data, we used a single archival pre-explosion *Spitzer* image to estimate and remove the galaxy background and nearby source contamination. We rotated and aligned IRAC images containing SN light based on the sky coordinates supplied in *Spitzer* data, and then simply subtract the archival image from a new science image. The location around SN 2004et is sufficiently sparse that careful PSF matching is not crucial. We conducted aperture photometry on the background-subtracted images and applied appropriate aperture corrections as given by the IRAC instrument handbook. We also estimated and removed residual background in the subtracted images using a sky aperture offset from the SN.

### 2.4 WISE archival photometry of SN 2004et

The location of SN 2004et was observed at several epochs during the ongoing NEOWISE all-sky, mid-IR survey in the W1 (3.4  $\mu\text{m}$ ) and W2 (4.6  $\mu\text{m}$ ) bands (Wright et al. 2010; Mainzer et al. 2014).

<sup>2</sup>[readthedocs.jhat.io](http://readthedocs.jhat.io)

<sup>3</sup><https://www.stsci.edu/hst/instrumentation/acs/data-analysis/aperture-corrections>

<sup>4</sup><https://www.stsci.edu/hst/instrumentation/wfc3/data-analysis/photometric-calibration/uvis-encircled-energy>

<sup>1</sup>[http://edd.ifa.hawaii.edu/get\\_cmd.php?pgc=65001](http://edd.ifa.hawaii.edu/get_cmd.php?pgc=65001)

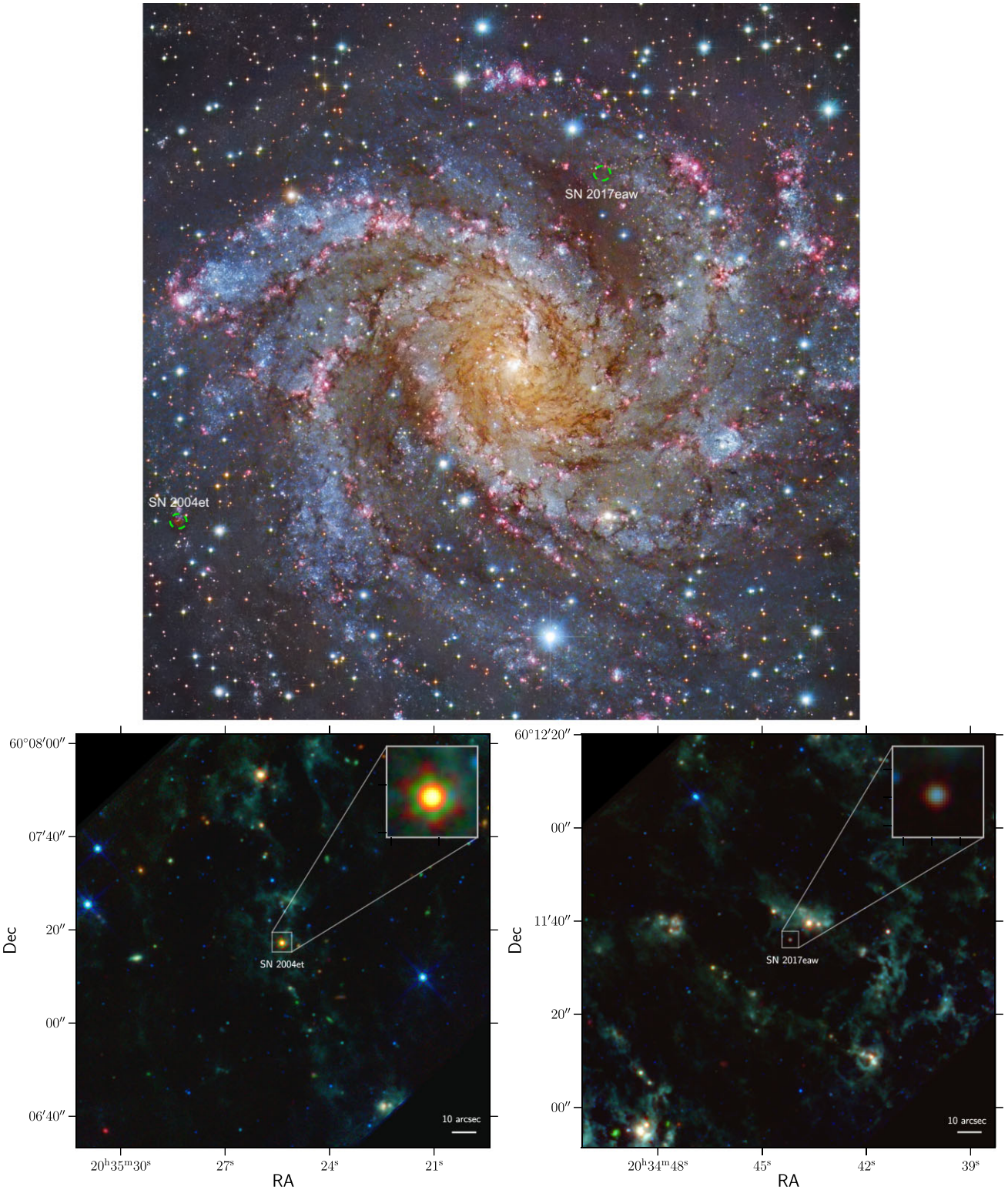


**Figure 1.** **Top panel:** *HST* image of NGC 6946, the host galaxy of both SNe 2004et and 2017eaw (courtesy of NASA, ESA, STScI, Gendler, and the Subaru Telescope). **Bottom left-hand panel:** Composite image of SN 2004et taken with *JWST*'s MIRI. **Bottom right-hand panel:** Composite image of SN 2017eaw taken with *JWST*'s MIRI. (MIRI filters used: F560W, F1000W, F1130W, F1280, F1500W, F1800W, F2100W, F2550W.).

**Table 1.** *JWST*/MIRI photometry<sup>1</sup>

Filters	SN 2004et		SN 2017eaw	
	Mag	Flux [ $\mu\text{Jy}$ ]	Mag	Flux [ $\mu\text{Jy}$ ]
F560W	$20.89 \pm 0.03$	$15.96 \pm 0.49$	$21.90 \pm 0.04$	$6.39 \pm 0.29$
F1000W	$18.67 \pm 0.01$	$122.63 \pm 1.51$	$19.49 \pm 0.01$	$58.12 \pm 0.79$
F1130W	$17.78 \pm 0.01$	$279.68 \pm 3.60$	$19.64 \pm 0.02$	$51.17 \pm 1.25$
F1280W	$17.25 \pm 0.01$	$456.39 \pm 4.36$	$19.81 \pm 0.01$	$43.30 \pm 0.58$
F1500W	$16.74 \pm 0.01$	$727.80 \pm 5.85$	$19.40 \pm 0.01$	$63.26 \pm 0.69$
F1800W	$16.36 \pm 0.01$	$1037.30 \pm 6.42$	$18.73 \pm 0.01$	$117.00 \pm 1.28$
F2100W	$16.16 \pm 0.01$	$1238.45 \pm 7.58$	$18.63 \pm 0.01$	$128.20 \pm 1.61$
F2550W	$15.75 \pm 0.01$	$1804.75 \pm 21.60$	$18.87 \pm 0.05$	$102.47 \pm 6.08$

<sup>1</sup>All observations were obtained on MJD 59842

We obtained the coadded time-series images of the fields created as part of the unWISE project (Lang 2014; Meisner, Lang & Schlegel 2018). A custom code (De et al. 2020) based on the ZOGY<sup>5</sup> image subtraction algorithm (Zackay, Ofek & Gal-Yam 2016) was used to perform image subtraction on the NEOWISE images using the full-depth coadds of the *WISE* and *NEOWISE* missions (obtained during 2010–2014) as reference images. Photometric measurements were obtained by performing forced PSF photometry at the transient position on the difference images until the epoch of the last *NEOWISE* data release (data acquired until 2021 December).

By mid-2017 ( $\sim 4500$  d post-discovery), SN 2004et had faded to a consistent flux below the zero-level of  $16 \pm 9$  and  $76 \pm 30$   $\mu\text{Jy}$  in the W1 and W2 difference images, respectively. This implies that SN emission was present in the 2010–2014 reference image coadd, and is largely consistent with the fluxes measured by *Spitzer* at those epochs in the similar 3.6- and 4.5- $\mu\text{m}$  IRAC bands. We thus offset the difference measurements by these values to obtain absolute flux estimates, though this yields no positive detections of the SN ( $> 3\sigma$ ) after 2014.

## 2.5 Optical spectroscopy

Late-time spectra of SNe 2004et and 2017eaw were obtained with the Keck Low Resolution Imaging Spectrometer (LRIS; Oke et al. 1995) on days 6424 and 1811, respectively (Fig. 2). The spectra were acquired with the slit oriented at or near the parallactic angle to minimize slit losses caused by atmospheric dispersion (Filippenko 1982). The LRIS observations utilized the 1-arcsec slit, 600/4000 grism, and 400/8500 grating. Data reduction followed standard techniques for CCD processing and spectrum extraction (Silverman et al. 2012) utilizing IRAF<sup>6</sup> (Tody 1986) routines and custom PYTHON and IDL codes.<sup>7</sup> The most recent LRIS spectra (from 2017 and later) were processed using the LPipe data-reduction pipeline (Perley 2019). Low-order polynomial fits to comparison-lamp spectra were used to calibrate the wavelength scale, and small adjustments derived from night-sky lines in the target frames were applied. The spectra were flux calibrated using observations of appropriate spectrophotometric standard stars observed on the same night, at similar airmasses, and with an identical instrument configuration.

<sup>5</sup><https://github.com/pmvreeswijk/ZOGY>

<sup>6</sup>IRAF is written and supported by the National Optical Astronomy Observatories, operated by the Association of Universities for Research in Astronomy, Inc. under cooperative agreement with the National Science Foundation.

<sup>7</sup><https://github.com/ishivvers/TheKastShiv>

## 3 ANALYSIS

### 3.1 Physical scenarios

Late-time thermal-IR continuum emission typically indicates the presence of dust. The general SN environment can be complicated, with many different possible origins and heating mechanisms for the dust (Fig. 3). The dust may be newly formed or pre-existing at the time of the SN. If newly formed, the dust may condense in the expanding SN ejecta (Kozasa, Hasegawa & Nomoto 1989; Wooden et al. 1993) or in the cool dense shell of post-shocked gas lying in between the forward and reverse shocks (Smith, Foley & Filippenko 2008). If pre-existing, the dust may have formed in a steady wind or during a short duration pre-SN outburst. In any scenario, several heating mechanisms are possible, including a thermal light echo from the peak SN flash, radiative heating from circumstellar interaction, and/or collisional heating by hot gas in the reverse shock (e.g. Fox et al. 2010). While strong CSM interaction that yields a Type II event is not typically associated with SNe IIP given the low density, relatively low mass-loss rates of their progenitor stars' winds ( $10^{-6} M_{\odot} \text{yr}^{-1}$ ; Beasor et al. 2020), it was more recently showed that even modest winds can build up and result in a relatively large ultraviolet (UV) flux at late times (Dessart & Hillier 2022; Dessart et al. 2023).

### 3.2 Corresponding dust models

In the optically thick case, the actual dust mass  $M_{\text{dust}}$  is related to the observationally inferred dust mass,  $M_{\text{dust}}^{\text{obs}}$ , by (Fox et al. 2010; Dwek et al. 2019)

$$M_{\text{dust}} = \frac{M_{\text{dust}}^{\text{obs}}}{P_{\text{esc}}(\tau)}, \quad (1)$$

where

$$M_{\text{dust}}^{\text{obs}} = \frac{F_{\lambda}^{\text{obs}}(\lambda) d^2}{B_{\lambda}(\lambda, T_{\text{dust}}) \kappa(\lambda)} \quad (2)$$

and  $F_{\lambda}^{\text{obs}}(\lambda)$  is the specific flux,  $d$  the distance to the source,  $\kappa(\lambda)$  is the dust mass absorption coefficient,  $B_{\lambda}(\lambda, T_{\text{dust}})$  is the Planck function at wavelength  $\lambda$ ,  $T_{\text{dust}}$  is the dust temperature, and  $P_{\text{esc}}$  is the escape probability of the infrared photons from the emitting region.

As described by Cox & Mathews (1969) and Osterbrock & Ferland (2006),  $P_{\text{esc}}$  is a function of optical depth ( $\tau$ ). For a homogeneous dusty sphere in which the absorbers (dust) are uniformly mixed with the emitting sources (in this case dust as well) is given by<sup>8</sup>

$$P_{\text{esc}}(\tau) = \frac{3}{4\tau} \left[ 1 - \frac{1}{2\tau^2} + \left( \frac{1}{\tau} + \frac{1}{2\tau^2} \right) e^{-2\tau} \right]. \quad (3)$$

The parameter  $\tau$  is a typical optical depth, which depends on the geometry of the emitting dust. Assuming that the dust in the SN ejecta can be approximated by a homogeneously expanding sphere, we get that

$$\begin{aligned} \tau(\lambda, t) &= \rho_{\text{dust}}(t) R(t) \kappa(\lambda) = \frac{3}{4} \left( \frac{M_{\text{dust}}(t)}{\pi R(t)^2} \right) \kappa(\lambda) \\ &= \frac{3}{4} \left( \frac{M_{\text{dust}}(t)}{\pi v_{\text{ej}}^2} \right) \kappa(\lambda) t^{-2} \end{aligned} \quad (4)$$

where  $\rho_{\text{dust}}(t)$  is the ejecta density,  $M_{\text{dust}}(t)$  is the total mass of ejecta dust,  $R(t)$  is the ejecta radius at time  $t$ , and  $v_{\text{ej}}$  is the ejecta velocity.

<sup>8</sup>The  $\lambda$  and time dependence of  $\tau$  has been suppressed for the sake of clarity.

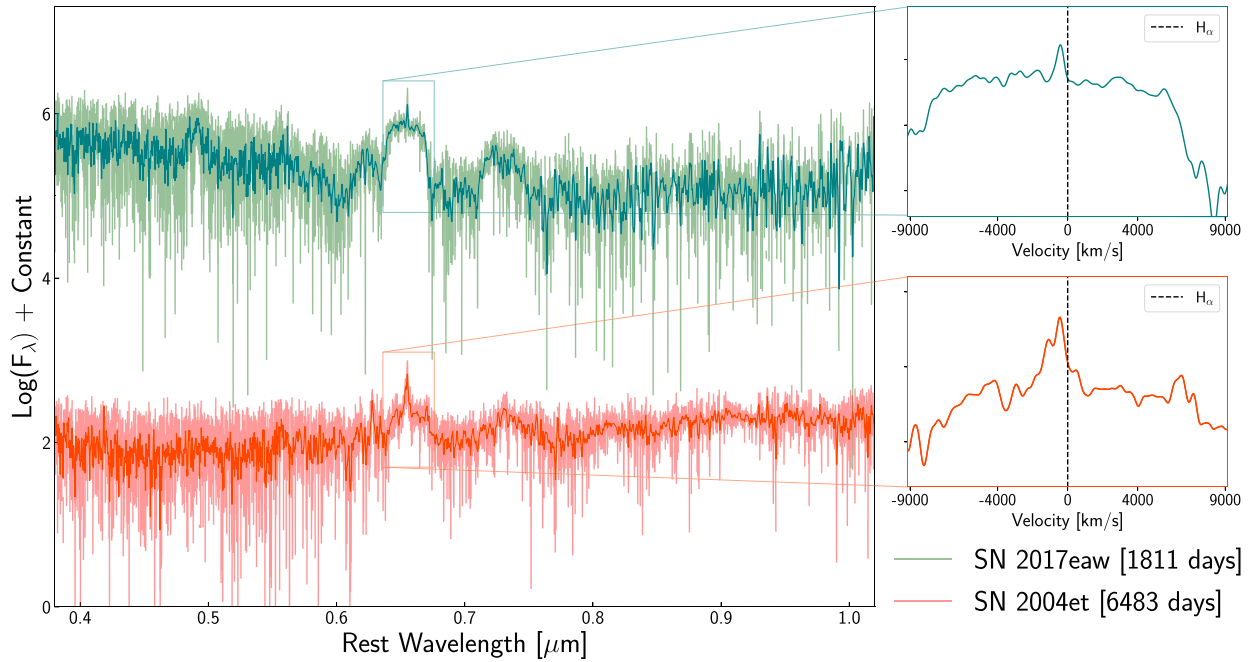


**Figure 2.** Late-time spectra of SNe 2004et and 2017eaw were obtained with the LRIS on days 6424 and 1811, respectively. The presence of the H $\alpha$  line signifies ongoing shock interaction with a pre-existing CSM.

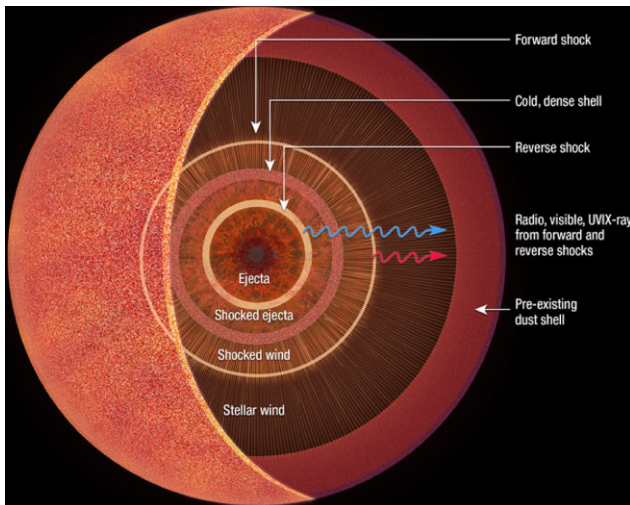


**Figure 3.** Illustration of how the dusty SN environment is relevant to our understanding of the SN explosion and progenitor taken from a number of papers (e.g. Fox et al. 2010, and those within). The dust may be newly formed in the ejecta or a cool, dense shell behind the forward shock. It may also be pre-existing as a circumstellar shell formed by pre-SN mass-loss from the progenitor star. The dust may be directly heated or radiatively heated by optical, UV, and X-ray emission from the shock. Disentangling all of these possibilities can constrain the origin of dust in the Universe and the late-stages of massive star evolution.

As a reference,  $1 M_{\odot}$  of ejecta dust expanding at a velocity of  $5000 \text{ km s}^{-1}$  will have a radial optical depth of  $\approx 6$  at  $20 \mu\text{m}$  after 10 yr of expansion, where we adopted a value of  $\kappa \approx 300 \text{ cm}^2 \text{ g}^{-1}$ , which is applicable for both silicates or amorphous carbon dust. So *a priori*, we cannot rule out the possibility that a large amount of dust may be hidden because of optical depth effects.

We can also calculate a *maximum* optical depth by assuming that the radiating dust is homogeneously distributed over the minimally allowed radius, given by the radius,  $R_{\text{BB}}$ , derived by assuming that the observed flux emanates from a perfect blackbody

$$R_{\text{BB}}(t) = \sqrt{\frac{L}{4\pi\sigma T^4}} = \sqrt{\frac{4\pi d^2 \int F_{\lambda}^{\text{obs}} d\lambda}{4\pi\sigma T^4}} \quad (5)$$

For values of  $R_{\text{BB}} \approx 5 \times 10^{16} \text{ cm}$ , we get a maximum  $20 \mu\text{m}$  optical depth of 60.

### 3.3 Fitting the data

To fit the IR data, we need to make some estimation about the dust composition. Since we do not have a mid-IR spectrum to base our assumptions, our choice of the chemical nature of dust is unconstrained. The many different chemical forms of cosmic dust relevant for SNe and their optical properties were explored by Arendt et al. (2014). In a simplified picture, observations and models of dust formation in SN ejecta, both support the presence of O-rich dust species in the form of Mg-silicates, and C-rich dust species such as amorphous carbon or graphite (Ercolano, Barlow & Sugerman 2007; Sarangi & Cherchneff 2013; Wesson & Bevan 2021). In this study, we have also chosen Mg-silicates and/or amorphous carbon as our dust composition. The absorption and emission properties of these grains are obtained from Draine & Li (2007) and Zubko, Dwek & Arendt (2004) for silicates and amorphous carbon, respectively [see Sarangi (2022) for the values of absorption coefficients  $\kappa$ ]. Given that we are dealing with mid-IR data, the wavelengths are much larger than the expected sizes of grains; in this Rayleigh regime, grain sizes do not impact the emerging fluxes. We have chosen the absorption coefficients corresponding to a grain radius of  $0.1 \mu\text{m}$ .

Using equation (2), we simultaneously fit the dust mass, temperature, composition, and opacity. It is important to note that the best-fitting parameters are not necessarily the values that we report.

Traditionally, the extragalactic SN dust community has used some variation of equation (2) to fit the mid-IR dust component straightforwardly with least squares minimization (i.e. using a package like PYTHON's `lmfit`). This technique, however, can be misleading. For the case of an increasing optical depth, a significant degeneracy begins to develop. As outlined by Dwek et al. (2019), an almost infinite dust mass can fit the data because the emission from the dust simply does not escape. The fits quickly become unbounded. Furthermore, we have multiple dust components to our model. It is therefore not reasonable to estimate the error from the covariance matrix. Instead, we explicitly calculate the confidence intervals for variable parameters using `lmfit.conf_interval`.<sup>9</sup> Figs 4 and 5 show the best-fitting results. Tables 2 and 3 report the best-fitting parameters, while Table 4 reports our final dust masses as the values given by the 90 per cent confidence interval.

In fitting the model we assumed that all the dust radiates at the same temperature, justifying the use of equation (3) for  $P_{\text{esc}}$ . A more realistic scenario would be to adopt several analytical forms for the dust temperature gradient in the ejecta and use a simple radiative transfer model, such as the one used by Dwek & Arendt (2020) in modeling the emission from the galaxy Arp 220.

At first glance, SNe 2004et and 2017eaw appear to have different compositions, with SN 2017eaw having a strong 10- $\mu\text{m}$  silicate feature. This may be true, but it may also be due to optical depth effects. Notice that an optically thick silicate dust sphere also fits the SN 2004et data quite well given the 10- $\mu\text{m}$  feature is suppressed. From the photometry alone, it is too difficult to distinguish between models. We therefore report results for both compositions for SN 2004et.

For both SN 2004et and SN 2017eaw, the F560W filter showed an excess relative to the best-fitting model. In both cases, we therefore add an additional, hotter contribution that we attribute to the likely presence of hot dust, either newly formed or continuously heated by ongoing shock interaction. Given the contributions of this hot component in only a single *JWST* filter, we have relatively few constraints. For SN 2004et, the only other long-wavelength (i.e. mid-IR) data we have are the *Spitzer* and *WISE* archival data (Sections 2.3 and 2.4), shown in Fig. 6. *Spitzer* observations are available only through  $\sim 4000$  d, while all *WISE* data at epochs  $> 4000$  d are upper limits. The trend in the *Spitzer* data is unclear. Although the light curve may be steadily declining, it may also be on a plateau, which is not uncommon for SNe that have signatures of CSM interaction, although the *Spitzer* fluxes for SN 2004et were close to the instrumental detection limits (see e.g. Fox et al. 2011, 2013; Szalai et al. 2019, 2021). Fig. 6 shows the possible fluxes at the epoch of the *JWST* observations for either scenario. We assume a flux in the range 10–18  $\mu\text{Jy}$  as reasonable, which is consistent with the F560W MIRI observations. Given the limited constraints we have on this warm dust, we add a 1000 K graphite component to both models.

In addition to the warm component in SN 2004et, we see an additional rise in the F2550W data point above the expected dust model fit. We attribute this flux to the presence of yet another dust component, this time much colder. Such a cold dust component is not unexpected, given that the majority of dust is expected to cool to temperatures  $< 40$  K, as it did in SN 1987A (Matsuura et al. 2011). Again, given the lack of data, we have few constraints. However, we vary the mass and temperature of this additional component and

show that significant quantities of dust may be present at these longer wavelengths.

## 4 DISCUSSION

### 4.1 Dust mass lower limits

It is worth repeating that the dust masses reported here are lower limits. We cannot account for dust hidden by high optical depths or cold dust emitting at wavelengths  $> 25$   $\mu\text{m}$ . Even when taking into account these lower limits, the dust mass observed in SN 2004et is still the second-largest measured dust mass based on mid-IR observations reported in any extragalactic SN to date. And aside from SN 1987A, the detections of dust in both SNe also correspond to the latest detections thus far of dust in any extragalactic SNe.

It is tempting to conclude an apparent trend of increasing dust mass with time in Fig. 7, but two important caveats should be noted. First, the dust origin and even heating mechanism is not straightforward. Section 4.2 explores the different possibilities. Secondly, the dust masses derived in previous studies are not consistent. The data sets range in mid-IR wavelength coverage and sensitivity, and the analysis techniques vary in scope, particularly how they report the best-fitting parameters versus the lower limits derived from the confidence intervals. Previous SEDs should be remodeled with a single, consistent procedure, but that work is beyond the scope of this paper.

### 4.2 Dust origin and heating mechanisms

The origin and intensity of the IR emission depend on the source that heats the dust, and the geometry of the dust distribution. As noted in Section 3.1, the dust may be pre-existing in the unshocked CSM, or newly formed either in the ejecta or in the swept up shell of gas behind the SN blastwave. Assuming the distribution to be isotropic, we can impart necessary constraints on the geometry that are consistent with the physical scenarios introduced in Section 3.1. Assuming the dust to be confined within a dusty sphere, the blackbody radius, given by equation (5), provides the smallest possible radius of the observed dust. For SN 2004et and SN 2017eaw, equation (5) yields a blackbody radius of  $\sim 5.4 \times 10^{16}$  and  $1.6 \times 10^{16}$  cm, respectively.

The dust formation zone within the metal-rich ejecta is expected to be confined within  $5000 \text{ km s}^{-1}$  (Truelove & McKee 1999; Maguire et al. 2012; Sarangi 2022), which is consistent with the velocity profile in Fig. 2. These velocities correspond to a radius of  $\sim 2.8 \times 10^{17}$  and  $7.8 \times 10^{16}$  cm for SN 2004et and SN 2017eaw, respectively. The ejecta radii are much larger than the blackbody radii; hence, the metal-rich ejecta is a completely acceptable site for dust that is responsible for the IR emission.

In the case of SN 2004et, Kotak et al. (2009) and Fabbri et al. (2011) have already done a detailed analysis on earlier optical and IR data that show increasing extinction over time that is consistent with new dust formation in the ejecta within the first 1000 d these same lines, the optical spectra in Fig. 2 show blueshifted  $\text{H}\alpha$  lines that are also consistent with dust present in the ejecta, that can preferentially absorb emission from the receding shock on the far side of the SN (Niculescu-Duvaz et al. 2022). In a spherical geometry pre-existing dust, which is present beyond the blastwave radius cannot lead to this blueshift in emission lines; therefore, we argue that the dust responsible for the IR emission is most likely newly formed.

In SNe IIP, which are characterized by RSG type pre-explosion mass-loss (typically of the order of  $10^{-6} M_{\odot} \text{ yr}^{-1}$ ), the swept up mass of gas by the SN blastwave in its first couple of decade after explosion

<sup>9</sup><https://lmfit.github.io/lmfit-py/confidence.html>



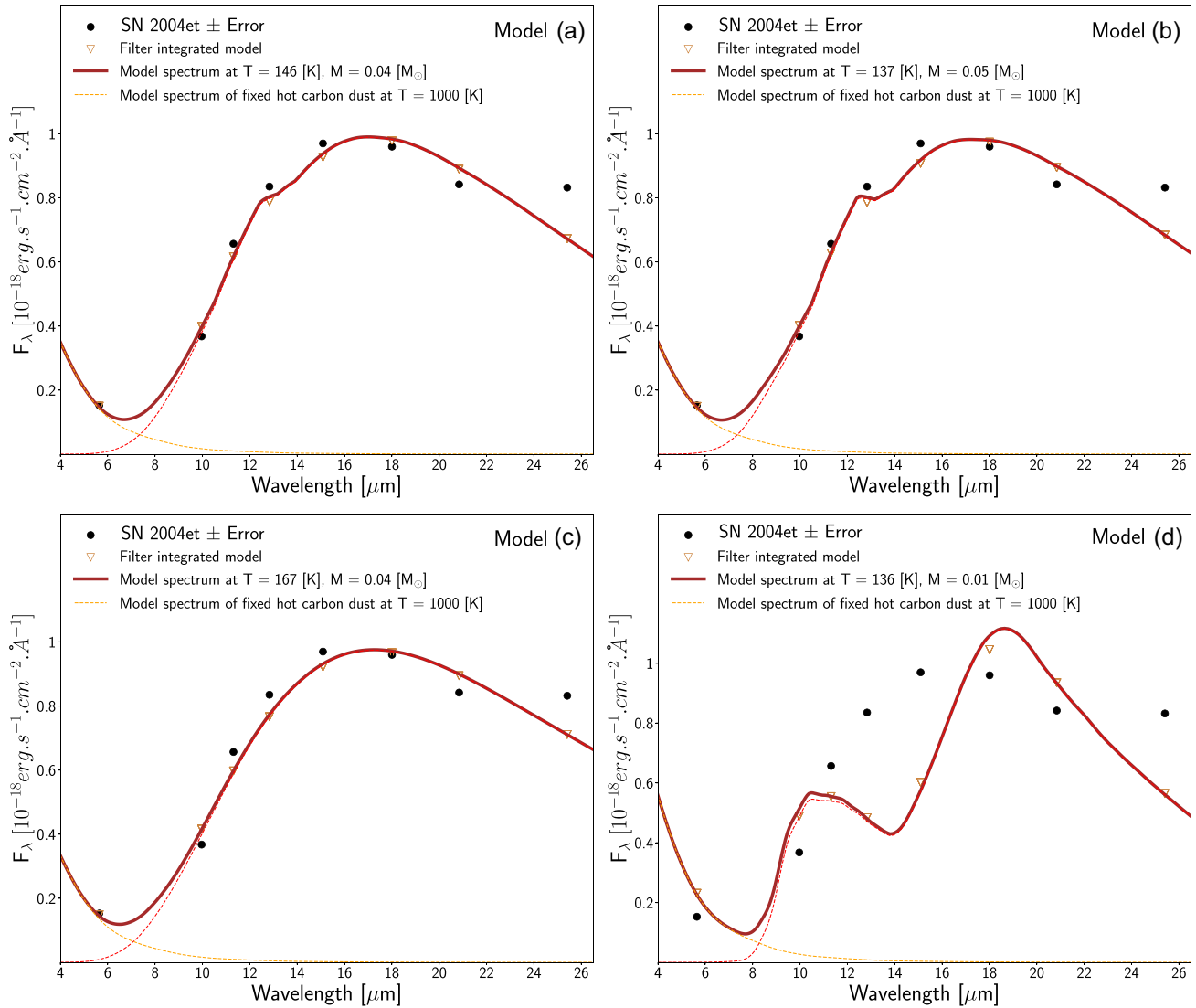


**Figure 4.** The MIR Spectral Energy Distribution (SED) of SN 2004et obtained with *JWST*/MIRI on 2022 September 20, fitted with different models/assumptions. For all four models, the solid line shows the model spectrum of amorphous C or silicates dust comprising two components. The orange dashed line shows a hot C component fixed at a temperature of 1000 K for all four scenarios, and the red dashed line shows the main C component. The resulting parameters are listed in Table 2. **Model (a)** is assuming a dusty sphere of amorphous C using equations (1) and (4), **Model (b)** shows an optically thin amorphous C dust using equation (1) with  $P_{\text{esc}} \approx 1$ , **Model (c)** is assuming a dusty sphere of silicates using equations (1) and (4), and **Model (d)** is an optically thin silicates dust using equation (1) with  $P_{\text{esc}} \approx 1$ .

should not exceed  $0.1 M_{\odot}$ . This circumstellar gas is typically H-rich, with refractory elements only amounting to about 1 percent. The CSM gas behind the shock is not likely to be the site that can produce the relatively large dust masses given in Tables 2 and 3.

Based on these arguments, the geometry favors the dust to be present in the ejecta. However, the time frame of the dust formation within the ejecta remains unclear. With only a limited number of data points, it is not possible to differentiate between a steady, continuous formation (e.g. Wesson & Bevan 2021), and a relatively rapid formation followed by years of increasing optical depth as the ejecta expand (Dwek et al. 2019). Higher cadence observations of future dust-forming SNe should be able to disentangle the two models.

To help constrain the scenario in either case, we must also identify the heating mechanism. In the first couple of years after the explosion, newly formed dust in the ejecta is understood to be heated by

the diffuse energy deposited in the ejecta, owing to the decay of radioactive  $^{56}\text{Co}$ . After 1500 d, the radioactive energy is dominated by the decay of  $^{44}\text{Ti}$  and possibly  $^{57}\text{Co}$  and  $^{60}\text{Co}$ ; however, their total luminosity is expected to not exceed  $10^3 L_{\odot}$  (Seitenzahl, Timmes & Magkotsios 2014). In this study, we find that the mid-IR fluxes of SN 2004et and SN 2017eaw correspond to the total luminosity of  $\sim 2.2 \times 10^5 L_{\odot}$  and  $3.2 \times 10^4 L_{\odot}$ , respectively. Therefore, there must be some additional source of energy that is heating the dust.

One source of heating is radiative emission from shock interaction. At sufficiently late times, interaction with a steady-state wind will always win against the exponential decline of radioactive decay power. Simulations by Dessart & Hillier (2022) find that a wind mass-loss rate of even  $10^{-6} M_{\odot} \text{ yr}^{-1}$  generates a constant shock power of about  $10^{40} \text{ erg s}^{-1}$  in a standard SN II. A fraction of that power will come out as X-rays. The thermalized part of this power

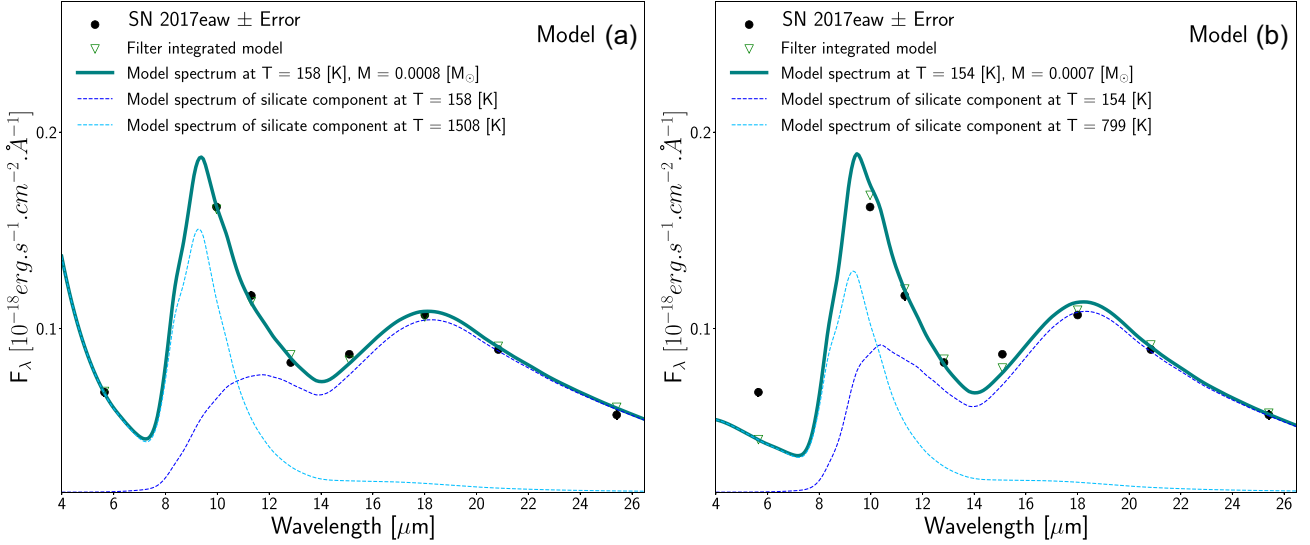


**Figure 5.** The MIR SED of SN 2017eaw obtained with *JWST*/MIRI on 2022 September 21, fitted with two different models/assumptions. For both models, the solid line shows the model spectrum of silicates dust comprising two components. The dashed lines show the two components. The resulting parameters are listed in Table 3. **Model (a)** is assuming a dusty sphere of silicates using equations (1) and (4), and **Model (b)** shows an optically thin silicate dust using equation (1) with  $P_{\text{esc}} \approx 1$ .

**Table 2.** Best-fitting dust model parameters for SN 2004et.

Model	$M_{\text{dust}}^a$ [ $M_{\odot}$ ]	$T^a$ [K]	$R^a$ [cm]	$\tau^b$	$P_{\text{esc}}^b$
(a) Dusty sphere (amorphous C)	$0.044^{+0.007}_{-0.007}$	$146^{+20}_{-10}$	$1.19^{+0.03}_{-0.63} \times 10^{17}$	$0 < \tau < 4.1$	$0.17 < P_{\text{esc}} < 1$
(b) Optically thin dust (amorphous C)	$0.047^{+0.007}_{-0.006}$	$137^{+3}_{-3}$	–	$\ll 1$	$\approx 1$
(c) Dusty sphere (silicates)	$0.036^{+0.012}_{-0.012}$	$167^{+5}_{-5}$	$5.24^{+0.46}_{-0.42} \times 10^{16}$	$8.9 < \tau < 29.7$	$0.02 < P_{\text{esc}} < 0.08$
(d) Optically thin dust (silicates)	$0.012^{+0.008}_{-0.005}$	$136^{+10}_{-10}$	–	$\ll 1$	$\approx 1$

<sup>a</sup> The numbers reported here are the best fit  $\pm$  the  $1\sigma$  (68 per cent) confidence interval as reported by `lmfit.conf.interval`. See Table 4 for final reported numbers.

<sup>b</sup>  $\tau$  and  $P_{\text{esc}}$  values have been calculated at the largest flux value ( $\lambda \approx 16 \mu\text{m}$ ).

**Table 3.** Best-fitting dust model parameters for SN 2017eaw.

Model	$M_{\text{dust}}^a$ [ $M_{\odot}$ ]	$T_{\text{hot}}^a$ [K]	$T_{\text{cold}}^a$ [K]	$R$ [cm]	$\tau^b$	$P_{\text{esc}}^b$
(a) Dusty sphere (silicates)	$0.0007^{+0.0004}_{-0.0002}$	$1508 \pm 793$	$158^{+5}_{-5}$	$2.87^{+2.92}_{-0.61} \times 10^{16}$	$0 < \tau < 0.8$	$0.6 < P_{\text{esc}} < 1$
(b) Optically thin dust (silicates)	$0.0006^{+0.0003}_{-0.0002}$	$800 \pm 521$	$154^{+12}_{-12}$	–	$\ll 1$	$\approx 1$

<sup>a</sup> The numbers reported here are the best fit  $\pm$  the  $1\sigma$  (68 per cent) confidence interval as reported by `lmfit.conf.interval`. See Table 4 for final reported numbers.

<sup>b</sup>  $\tau$  and  $P_{\text{esc}}$  values have been calculated at  $\lambda \approx 18 \mu\text{m}$ .

**Table 4.** Reported dust properties.

SN	$M_{\text{dust}}^a$ [ $M_{\odot}$ ]	$R_{\text{BB}}$ [cm]	$R_{\text{shock}}$ [cm]	$L_{\text{IR}}$ [ $L_{\odot}$ ]	$L_{\text{opt}}$ [ $L_{\odot}$ ]
SN 2004et (C)	$>0.033$	$5.4 \times 10^{16}$	$2.8 \times 10^{17}$	$2.2 \times 10^5$	$1.4 \times 10^4$
SN 2004et (Sil)	$>0.014$	$5.4 \times 10^{16}$	$2.8 \times 10^{17}$	$2.2 \times 10^5$	$1.4 \times 10^4$
SN 2017eaw (Sil)	$>4 \times 10^{-4}$	$1.6 \times 10^{16}$	$7.8 \times 10^{16}$	$3.2 \times 10^4$	$1.3 \times 10^4$

<sup>a</sup> With 90 per cent confidence using `lmfit.conf.interval`.

will emerge primarily in the UV, especially in  $\text{Ly}\alpha$  1215.67 Å and  $\text{Mg II}$  2800 Å, while a few per cent of that thermalized flux emerges in the optical as a weak continuum source together with emission lines, in particular  $\text{H}\alpha$ .

We know that both SNe 2004et and 2017eaw are undergoing late-time CSM interaction. Fig. 2 plots the most recent optical spectra. Strong rebrightening in the Spitzer CH1 and CH2 light curves of SN 2004et (Fig. 6) around 1000 d after explosion is explained by the impact of the ejecta on the progenitor CSM, leading to dust formation in the cool dense shell (CDS; Kotak et al. 2009; Fabbri et al. 2011). This rebrightening phase seems to end within a few hundred days (Fig. 6); thus, it is unlikely that it directly connects to *JWST* measurements obtained years later. However, we cannot rule out the possibility that the *JWST* mid-IR dust could have been formed during that same rebrightening phase and has cooled down. The integrated flux for the late-time optical spectra of SNe 2004et and 2017eaw corresponds to only about  $\sim 10^4 L_{\odot}$  (Fig. 4). The

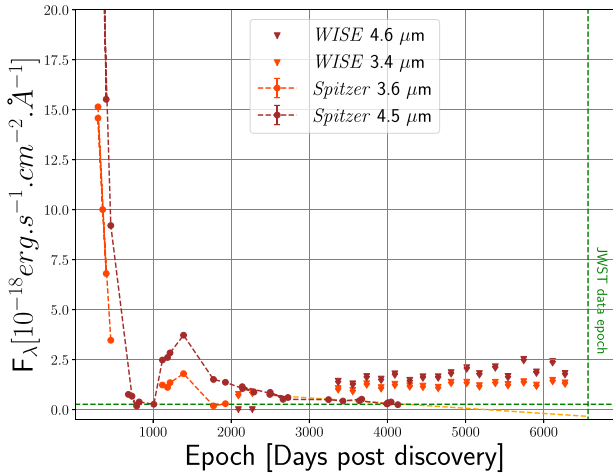


**Figure 6.** *Spitzer* and *WISE* photometry of SN 2004et. These data were all obtained at much earlier epochs, but help serve as a useful constraint on the presence of a hot component we use in our SN 2004et models in Fig. 4. Note that *WISE* fluxes shown here are upper limits.

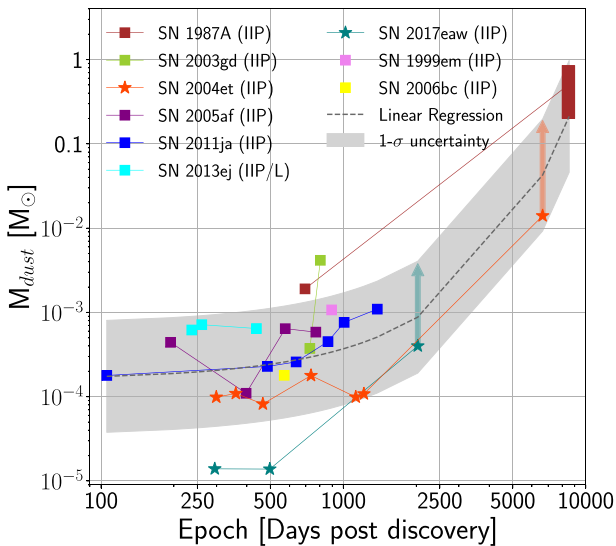


**Figure 7.** The dust mass in SN, as inferred from observations using the optically thin approximation, as a function of the epoch of observations. The trend may either suggest the growth of dust mass, or the increasing transparency of the ejecta with time. The vertical arrows for both SNe 2004et and 2017eaw show the possible dust reservoirs in these SNe based on our SED fits.

observed optical luminosity is not sufficient to heat the dust, but it does not represent the total luminosity produced by the shock–CSM interaction. Dessart & Hillier (2022) shows that the shock power introduced at the interface between ejecta and CSM emerges primarily in the UV, channeled primarily into  $\text{Ly}\alpha$ , for which we have no observational coverage, even in the archival *HST*/WFC3 UVIS data. These models suggest that the observed optical luminosities ( $\sim 10^4 L_{\odot}$ ) could be compatible with a UV flux of  $\sim 10^5 L_{\odot}$ , which is more than sufficient to heat the dust to the observed temperature and luminosity.

To summarize, we propose that the most plausible scenario is that the dust is present in the ejecta, and is being heated by the

interaction between the SN forward shock and the ambient CSM. Since the heating source of the dust (that is, the forward shock) is external to the ejecta dust in a spherical geometry, it is not possible to find the exact radius of the dusty sphere despite knowing the dust temperatures, as the laws of electrostatics state that the field strength is uniform inside a sphere. The percentage of the forward shock luminosity incident on the ejecta dust depends on the ratio of velocities between the outer radius of the metal-rich ejecta and the forward shock. Owing to the very large absorption coefficient of both amorphous carbon and silicates in the UV bands (Sarangi 2022), the lower limit of the dust mass (derived in this study) is sufficient to completely absorb the incident radiation from the forward shock [can be verified by equation (3)]. On the contrary, the optical depths are much lower in the mid-IR bands, where we probe the SNe with *JWST*. Therefore, we can expect that all the absorbed radiation will be reprocessed and radiated back in the IR. For SN 2004et, using the IR luminosity of  $2.2 \times 10^5 L_{\odot}$  and a dust temperature of  $\sim 140$  K, if we assume equilibrium of absorption and emission (Temim & Dwek 2013; Sarangi 2022), the approximate forward shock velocity can be calculated to be  $\sim 10\,000 \text{ km s}^{-1}$ . Comparing the IR luminosity to the forward shock luminosity (which is expected to be at least  $10^{40} \text{ erg s}^{-1}$ , suggested by Dessart & Hillier 2022), the velocity of the dusty ejecta can be found estimated as  $\sim 3000 \text{ km s}^{-1}$ , which matches well with the location of carbon-dust formation (Sarangi 2022).

Interestingly, we find that the total IR luminosity of SN 2004et is higher than the luminosity of SN 2017eaw, even though the latter is younger and is expected to have a stronger forward shock luminosity. This may indicate that the younger SN 2017eaw, being more compact, is optically thick in the mid-IR, as some theoretical studies suggest (Dwek et al. 2019; Sarangi 2022). On the other hand, it may also indicate that the silicate-rich dust in the ejecta of SN 2017eaw is expanding at a smaller velocity (compared to carbon dust in SN 2004et), so a smaller fraction of the forward shock luminosity is absorbed here. This is again in agreement with theoretical models, which predict that silicate dust is formed in the inner regions (hence smaller velocity) of the metal-rich ejecta (Sarangi et al. 2018).

We did not factor the impact of clumpiness of the ejecta in our analysis. The optical depths are expected to be lower in the case of clumpy ejecta (Inoue et al. 2020). Therefore, the lower limit on the dust mass that we estimated from an optically thin scenario in this study remains completely valid. The escape probabilities of the UV photons, and therefore the heating rates, might alter when clumpiness is taken into account. We intend to address the impact of clumpiness in a future study, when more data are available to constrain our results.

Other possible scenarios exist for the heating of the dust. For example, the majority of the flux may actually come out in X-rays at late times. The reverse shock may have traveled sufficiently far back into the ejecta to be heating them directly (i.e. not radiatively). The optical depth is quite high, thereby absorbing 99 percent of the optical flux. Or there may be a pulsar at the centre. Each of these scenarios requires additional observations and more complex models, all of which are beyond the scope of this paper.

## 5 CONCLUSION

In this article, we present *JWST* MIRI observations of SNe 2004et and 2017eaw at roughly 18 and 5 yr post-explosion, respectively. The mid-IR imaging unveils reservoirs of warm dust totaling  $>0.014$  and  $>4 \times 10^{-4} M_{\odot}$ , respectively. When compared to other mid-IR observations of dust in SNe, these are some of the latest detections

and highlight the sensitivity of *JWST*. Aside from SN 1987A, SN 2004et has the largest mid-IR inferred dust mass of any extragalactic SN to date. The results extend the empirical trend of an increasing dust mass in SNe IIP at late times. Even at day  $\sim 6500$ , the dust in SN 2004et is still opaque ( $\tau > 1$ ), allowing for the possibility that even more dust could be detected as the ejecta continue to expand. This trend suggests that we may be able to detect  $> 1 M_{\odot}$  of dust in extragalactic SNe at  $> 10\,000$  d, which would be sufficient to account for dust in the early universe (Dwek et al. 2007) if it can survive the reverse shock and injection back into the Universe (Slavin et al. 2020).

Despite the new discoveries made available by this extraordinary photometric data set, there are still several caveats. For instance, the overall fits have a range of possible models, reflected in the confidence intervals in Tables 2 and 3. We report a lower limit for our dust mass derivation, but most dust compositions and optical depths will actually result in a larger inferred dust mass. The MIRI Medium Resolution Spectrograph (MRS) can help to tighten these constraints and perhaps even differentiate between optically thin and thick dust models.

Along these same lines, MIRI is only mostly sensitive to the warm dust. There appear to be both hotter and colder components contributing at shorter and longer wavelengths. Regardless of the confidence intervals, the dust masses reported here should therefore be considered only as lower limits. While near-IR instruments can provide shorter-wavelength data, no instruments offer longer-wavelength data. MRS, again, can offer useful constraints of the colder dust component at the longest wavelengths by providing the shape of the long-wavelength curve. Also, optical data are needed to examine the interaction of the shock with the circumstellar dust and gas.

The blackbody radius provides only a minimum dust radius, and we rely on this as one of our arguments for the dust originating in the ejecta. Of course, the dust shell may be much larger, asymmetric, or clumpy. Detailed radiative-transfer modeling beyond the scope of this work must take into account these possibilities to provide consistency between the dust temperature, geometry, and heating mechanism. The heating mechanism is another unknown; in our case, the optical luminosity is insufficient to power the dust to the observed luminosity. We assume a UV component from theoretical models, but these models are untested. No SN IIP has ever been observed at  $\text{Ly}\alpha$  at late times. *HST* spectroscopy at these wavelengths could confirm the heating mechanism. If  $\text{Ly}\alpha$  emission is not present, other possibilities must be explored, as discussed in the text.

Finally, the observed empirical trend implies significant dust growth over decades, but this trend only corresponds to the *inferred* dust growth. The actual dust growth may have happened at early times, with progressively more dust visible as the ejecta expand and become increasingly optically thin. Testing dust formation and evolution scenarios requires continued monitoring at multiple wavelengths. In other words, more observations are required to explore this new, exciting field of dusty SNe in the era of *JWST*.

## ACKNOWLEDGEMENTS

This work is based on observations made with the NASA/ESA/CSA *James Webb Space Telescope (JWST)*. The data were obtained from the Mikulski Archive for Space Telescopes at the Space Telescope Science Institute, which is operated by the Association of Universities for Research in Astronomy, Inc., under NASA contract NAS 5–03127 for *JWST*. These observations are associated with programme #2666. Some of the data presented herein were obtained at the WM

Keck Observatory, which is operated as a scientific partnership among the California Institute of Technology, the University of California, and NASA; the observatory was made possible by the generous financial support of the WM Keck Foundation. A major upgrade of the Kast spectrograph on the Shane 3-m telescope at Lick Observatory, led by Brad Holden, was made possible through generous gifts from the Heising–Simons Foundation, William and Marina Kast, and the University of California Observatories. Research at Lick Observatory is partially supported by a generous gift from Google. AVF's supernova group at UC Berkeley is grateful for financial assistance from the Christopher R Redlich Fund and many individual donors. TS has been supported by the János Bolyai Research Scholarship of the Hungarian Academy of Sciences, as well as by the FK134432 grant of the National Research, Development and Innovation (NRDI) Office of Hungary and the ÚNKP 22–5 New National Excellence Programs of the Ministry for Culture and Innovation from the source of the NRDI Fund, Hungary. The research of YY has been supported through a Bengier–Winslow–Robertson Fellowship.

## DATA AVAILABILITY

All data are incorporated into the article and its online supplementary material.

## REFERENCES

- Anand G. S., Rizzi L., Tully R. B., 2018, *AJ*, 156, 105  
 Andrews J. E. et al., 2010, *ApJ*, 715, 541  
 Andrews J. E. et al., 2011, *AJ*, 142, 45  
 Arendt R. G., Dwek E., Kober G., Rho J., Hwang U., 2014, *ApJ*, 786, 55  
 Argo M., Torres M. P., Beswick R., Wrigley N., 2017, *Astron. Telegram*, 10472, 1  
 Beasor E. R., Davies B., Smith N., van Loon J. T., Gehrz R. D., Figer D. F., 2020, *MNRAS*, 492, 5994  
 Beswick R. J., Muxlow T. W. B., Argo M. K., Pedlar A., Marcaide J. M., 2004, *IAU Circ.*, 8435, 3  
 Bevan A., Barlow M. J., 2016, *MNRAS*, 456, 1269  
 Bevan A., Barlow M. J., Milisavljevic D., 2017, *MNRAS*, 465, 4044  
 Bevan A. et al., 2019, *MNRAS*, 485, 5192  
 Bose S., Kumar B., 2014, *ApJ*, 782, 98  
 Bouchet P. et al., 2015, *PASP*, 127, 612  
 Bright S. N., *JWST/MIRI Team*, 2016, in *American Astronomical Society Meeting Abstracts #227*. p. 147.15  
 Bushouse H. et al., 2022, *JWST Calibration Pipeline*, available at: <https://doi.org/10.5281/zenodo.7229890>  
 Buta R. J., Keel W. C., 2019, *MNRAS*, 487, 832  
 Cernuschi F., Codina S., 1967, *AJ*, 72, 788  
 Cherchneff I., Dwek E., 2009, *ApJ*, 703, 642  
 Chevalier R. A., Fransson C., Nymark T. K., 2006, *ApJ*, 641, 1029  
 Clayton D. D., Nittler L. R., 2004, *ARA&A*, 42, 39  
 Cox D. P., Mathews W. G., 1969, *ApJ*, 155, 859  
 Crockett R. M., Smartt S. J., Pastorello A., Eldridge J. J., Stephens A. W., Maund J. R., Mattila S., 2011, *MNRAS*, 410, 2767  
 De Looze I., Barlow M. J., Swinyard B. M., Rho J., Gomez H. L., Matsuura M., Wesson R., 2017, *MNRAS*, 465, 3309  
 De K. et al., 2020, *PASP*, 132, 025001  
 Dessart L., Hillier D. J., 2022, *A&A*, 660, L9  
 Dessart L., Gutierrez C. P., Kuncarayakti H., Fox O. D., Filippenko A. V., 2023, preprint ([arXiv:2301.09089](https://arxiv.org/abs/2301.09089))  
 Dong S., Stanek K. Z., 2017, *Astron. Telegram*, 10372, 1  
 Draine B. T., Li A., 2007, *ApJ*, 657, 810  
 Dwek E., Arendt R. G., 2020, *ApJ*, 901, 36  
 Dwek E., Galliano F., Jones A. P., 2007, *ApJ*, 662, 927  
 Dwek E., Sarangi A., Arendt R. G., 2019, *ApJ*, 871, L33

- Eldridge J. J., Xiao L., 2019, *MNRAS*, 485, L58
- Ercolano B., Barlow M. J., Sugerman B. E. K., 2007, *MNRAS*, 375, 753
- Fabbri J. et al., 2011, *MNRAS*, 418, 1285
- Fazio G. G. et al., 2004, *ApJS*, 154, 10
- Filippenko A. V., 1982, *PASP*, 94, 715
- Fox O. D., Chevalier R. A., Dwek E., Skrutskie M. F., Sugerman B. E. K., Leisenring J. M., 2010, *ApJ*, 725, 1768
- Fox O. D. et al., 2011, *ApJ*, 741, 7
- Fox O. D., Filippenko A. V., Skrutskie M. F., Silverman J. M., Ganeshalingam M., Cenko S. B., Clubb K. I., 2013, *AJ*, 146, 2
- Gall C., Hjorth J., Andersen A. C., 2011, *A&AR*, 19, 43
- Gall C. et al., 2014, *Nat.*, 511, 326
- Gerardy C. L., Fesen R. A., Nomoto K., Maeda K., Hoflich P., Wheeler J. C., 2002, *PASJ*, 54, 905
- Greenfield P., Miller T., 2016, *Astron. Comput.*, 16, 41
- Grefenstette B., Harrison F., Brightman M., 2017, *Astron. Telegram*, 10427, 1
- Herrmann K. A., Ciardullo R., Feldmeier J. J., Vinciguerra M., 2008, *ApJ*, 683, 630
- Hillier D. J., Dessart L., 2019, *A&A*, 631, A8
- Hosseinzadeh G. et al., 2023, *ApJ*, 942, L18
- Hoyle F., Wickramasinghe N. C., 1970, *Nat.*, 226, 62
- Indebetouw R. et al., 2014, *ApJ*, 782, L2
- Inoue A. K., Hashimoto T., Chihara H., Koike C., 2020, *MNRAS*, 495, 1577
- Jencson J. E. et al., 2019, *ApJ*, 886, 40
- Jerkstrand A., Fransson C., Maguire K., Smartt S., Ergon M., Spyromilio J., 2012, *A&A*, 546, A28
- Johnson S. A., Kochanek C. S., Adams S. M., 2018, *MNRAS*, 480, 1696
- Karachentsev I. D., Sharina M. E., Huchtmeier W. K., 2000, *A&A*, 362, 544
- Kasliwal M. M. et al., 2017, *ApJ*, 839, 88
- Kilpatrick C. D., Foley R. J., 2018, *MNRAS*, 481, 2536
- Kong A. K. H., Li K. L., 2017, *Astron. Telegram*, 10380, 1
- Kotak R. et al., 2009, *ApJ*, 704, 306
- Kozasa T., Hasegawa H., Nomoto K., 1989, *ApJ*, 344, 325
- Lang D., 2014, *AJ*, 147, 108
- Li W., Van Dyk S. D., Filippenko A. V., Cuillandre J.-C., 2005, *PASP*, 117, 121
- Maguire K. et al., 2010, *MNRAS*, 404, 981
- Maguire K. et al., 2012, *MNRAS*, 420, 3451
- Mainzer A. et al., 2014, *ApJ*, 792, 30
- Maiolino R., Schneider R., Oliva E., Bianchi S., Ferrara A., Mannucci F., Pedani M., Sogorb M. R., 2004, *Nat.*, 431, 533
- Martí-Vidal I. et al., 2007, *A&A*, 470, 1071
- Martinez L., Bersten M. C., 2019, *A&A*, 629, A124
- Matsuura M. et al., 2011, *Sci.*, 333, 1258
- Matsuura M. et al., 2015, *ApJ*, 800, 50
- Meikle W. P. S. et al., 2007, *ApJ*, 665, 608
- Meikle W. P. S. et al., 2011, *ApJ*, 732, 109
- Meisner A. M., Lang D. A., Schlegel D. J., 2018, *Res. Notes Am. Astron. Soc.*, 2, 202
- Misra K., Pooley D., Chandra P., Bhattacharya D., Ray A. K., Sagar R., Lewin W. H. G., 2007, *MNRAS*, 381, 280
- Morozova V., Piro A. L., Valenti S., 2018, *ApJ*, 858, 15
- Nagy A. P., Ordasi A., Vinkó J., Wheeler J. C., 2014, *A&A*, 571, A77
- Nayana A. J., Chandra P., 2017, *Astron. Telegram*, 10534, 1
- Niculescu-Duvaz M. et al., 2022, *MNRAS*, 515, 4302
- Nozawa T., Kozasa T., Umeda H., Maeda K., Nomoto K., 2003, *ApJ*, 598, 785
- Nozawa T. et al., 2008, *ApJ*, 684, 1343
- Oke J. B., Gunn J. E., 1983, *ApJ*, 266, 713
- Oke J. B. et al., 1995, *PASP*, 107, 375
- Osterbrock D. E., Ferland G. J., 2006, *Astrophysics of Gaseous Nebulae and Active Galactic Nuclei.*, CA Publisher, University Science Books
- Owen P. J., Barlow M. J., 2015, *ApJ*, 801, 141
- Perley D. A., 2019, *PASP*, 131, 084503
- Perrin M. D., Sivaramakrishnan A., Lajoie C.-P., Elliott E., Pueyo L., Ravindranath S., Albert L., 2014, in Oschmann J. M., Jr., Clampin M., Fazio G. G., MacEwen H. A. eds, *Proc. SPIE Conf. Ser. Vol. 9143, Space Telescopes and Instrumentation 2014: Optical, Infrared, and Millimeter Wave.* SPIE, Bellingham. p. 91433X
- Pozzo M., Meikle W. P. S., Fassia A., Geballe T., Lundqvist P., Chugai N. N., Sollerman J., 2004, *MNRAS*, 352, 457
- Priestley F. D., Barlow M. J., De Looze I., Chawner H., 2020, *MNRAS*, 491, 6020
- Ressler M. E. et al., 2015, *PASP*, 127, 675
- Rho J., Jarrett T. H., Chugai N. N., Chevalier R. A., 2007, *ApJ*, 666, 1108
- Rho J., Geballe T. R., Banerjee D. P. K., Dessart L., Evans A., Joshi V., 2018, *ApJ*, 864, L20
- Ricks W., Dwarkadas V. V., 2019, *ApJ*, 880, 59
- Rieke G. H., Lebofsky M. J., 1985, *ApJ*, 288, 618
- Rieke G., Wright G., 2022, *Nature Astron.*, 6, 891
- Rieke G. H. et al., 2015, *PASP*, 127, 584
- Rizzo Smith M., Kochanek C. S., Neustadt J. M. M., 2023, *MNRAS*, 523, 1474
- Rui L. et al., 2019, *MNRAS*, 485, 1990
- Sahu D. K., Anupama G. C., Srividya S., Muneer S., 2006, *MNRAS*, 372, 1315
- Sarangi A., 2022, *A&A*, 668, A57
- Sarangi A., Cherkneff I., 2013, *ApJ*, 776, 107
- Sarangi A., Cherkneff I., 2015, *A&A*, 575, A95
- Sarangi A., Matsuura M., Micelotta E. R., 2018, *Space Sci. Rev.*, 214, 63
- Schneider R., Ferrara A., Salvaterra R., 2004, *MNRAS*, 351, 1379
- Seitzzahl I. R., Timmes F. X., Magkotsios G., 2014, *ApJ*, 792, 10
- Silverman J. M. et al., 2012, *MNRAS*, 425, 1789
- Slavin J. D., Dwek E., Mac Low M.-M., Hill A. S., 2020, *ApJ*, 902, 135
- Sluder A., Milosavljević M., Montgomery M. H., 2018, *MNRAS*, 480, 5580
- Smith N., Foley R. J., Filippenko A. V., 2008, *ApJ*, 680, 568
- Stockdale C. J., Weiler K. W., van Dyk S. D., Sramek R. A., Panagia N., Marcaide J. M., 2004, *IAU Circ.*, 8415, 1
- Sugerman B. E. K. et al., 2006, *Sci.*, 313, 196
- Szalai T., Vinkó J., Balog Z., Gáspár A., Block M., Kiss L. L., 2011, *A&A*, 527, A61
- Szalai T. et al., 2019, *ApJ*, 876, 19
- Szalai T. et al., 2021, *ApJ*, 919, 17
- Temim T., Dwek E., 2013, *ApJ*, 774, 8
- Temim T., Dwek E., Arendt R. G., Borkowski K. J., Reynolds S. P., Slane P., Gelfand J. D., Raymond J. C., 2017, *ApJ*, 836, 129
- Tikhonov N. A., 2014, *Astron. Lett.*, 40, 537
- Tinyanont S. et al., 2016, *ApJ*, 833, 231
- Tinyanont S. et al., 2019, *ApJ*, 873, 127
- Todini P., Ferrara A., 2001, *MNRAS*, 325, 726
- Tody D., 1986, in Crawford D. L. ed., *Proc. SPIE Conf. Ser. Vol. 627, Instrumentation in Astronomy VI.* SPIE, Bellingham. p. 733
- Truelove J. K., McKee C. F., 1999, *ApJS*, 120, 299
- Tsvetkov D. Y. et al., 2018, *Astron. Lett.*, 44, 315
- Utrobin V. P., Chugai N. N., 2009, *A&A*, 506, 829
- van Dyk S. D. et al., 2019, *ApJ*, 875, 136
- van Dyk S. D., Filippenko A. V., Fox O. D., Kelly P. L., Milisavljevic D., Smith N., 2017, *Astron. Telegram*, 10378, 1
- Weil K. E., Fesen R. A., Patnaude D. J., Milisavljevic D., 2020, *ApJ*, 900, 11
- Wesson R., Bevan A., 2021, *ApJ*, 923, 148
- Wesson R., Barlow M. J., Matsuura M., Ercolano B., 2015, *MNRAS*, 446, 2089
- Wiggins P., 2017, *Transient Name Server Discovery Rep.*, 2017-548, 1
- Williams B. F., Hillis T. J., Murphy J. W., Gilbert K., Dalcanton J. J., Dolphin A. E., 2018, *ApJ*, 860, 39
- Wooden D. H., Rank D. M., Bregman J. D., Witteborn F. C., Tielens A. G. G. M., Cohen M., Pinto P. A., Axelrod T. S., 1993, *ApJS*, 88, 477
- Wright E. L. et al., 2010, *AJ*, 140, 1868
- Xue M., Jiang B. W., Gao J., Liu J., Wang S., Li A., 2016, *ApJS*, 224, 23
- Zackay B., Ofek E. O., Gal-Yam A., 2016, *ApJ*, 830, 27
- Zubko V., Dwek E., Arendt R. G., 2004, *ApJS*, 152, 211
- Zwitter T., Munari U., Moretti S., 2004, *Cent. Bur. Electron. Telegrams*, 95, 1

**SUPPORTING INFORMATION**

Supplementary data are available at [MNRAS](https://www.mnras.org) online.

**Figure S1.** Top panels: *HST* late-time light curve and SED of SN 2004et.

**Figure S2.** *WISE* photometry of SN 2017eaw.

**Figure S3.** Left-hand panel: Optical spectra of SN 2004et ranging from 4 to 6483 d post-discovery.

**Table S1.** *HST* Imaging of SN 2004et

**Table S2.** *HST* Imaging of SN 2017eaw

**Table S3.** *Spitzer* IRAC photometry of SN 2004et

**Table S4.** *WISE* Archival Imaging of SN 2004et

**Table S5.** *WISE* Archival Imaging of SN 2017eaw

Please note: Oxford University Press is not responsible for the content or functionality of any supporting materials supplied by the authors. Any queries (other than missing material) should be directed to the corresponding author for the article.

<sup>1</sup>*Department of Physics and Astronomy, Johns Hopkins University, Baltimore, MD 21218, USA*

<sup>2</sup>*Space Telescope Science Institute, 3700 San Martin Drive, Baltimore, MD 21218, USA*

<sup>3</sup>*DARK, Niels Bohr Institute, University of Copenhagen, Jagtvej 128, 2200 Copenhagen, Denmark*

<sup>4</sup>*Department of Astrophysical Sciences, Princeton University, Princeton, NJ 08544, USA*

<sup>5</sup>*Department of Experimental Physics, Institute of Physics, University of Szeged, H-6720 Szeged, Dóm tér 9, Hungary*

<sup>6</sup>*ELKH-SZTE Stellar Astrophysics Research Group, H-6500 Baja, Szegedi út, Kt. 766, Hungary*

<sup>7</sup>*Department of Astronomy and Astrophysics, University of California, Santa Cruz, CA 95064, USA*

<sup>8</sup>*Observational Cosmology Lab, NASA Goddard Space Flight Center, Code 665, Greenbelt, MD 20771, USA*

<sup>9</sup>*Institut d'Astrophysique de Paris, CNRS-Sorbonne Université, 98 bis boulevard Arago, F-75014 Paris, France*

<sup>10</sup>*Department of Astronomy, University of California, Berkeley, CA 94720-3411, USA*

<sup>11</sup>*Gemini Observatory, 670 N. Aohoku Place, Hilo, Hawaii, HI 96720, USA*

<sup>12</sup>*Department of Physics & Astronomy, Louisiana State University, Baton Rouge, LA 70803, USA*

<sup>13</sup>*MIT-Kavli Institute for Astrophysics and Space Research, 77 Massachusetts Ave., Cambridge, MA 02139, USA*

<sup>14</sup>*Department of Physics, The Oskar Klein Center, Stockholm University, AlbaNova, 10691 Stockholm, Sweden*

<sup>15</sup>*Cahill Center for Astrophysics, California Institute of Technology, 1200 E. California Blvd. Pasadena, CA 91125, USA*

<sup>16</sup>*NSF's NOIRLab, 950 N. Cherry Avenue, Tucson, 85719, AZ, USA*

<sup>17</sup>*Sterrenkundig Observatorium, Ghent University, Krijgslaan 281 - S9, 9000 Gent, Belgium*

<sup>18</sup>*European Space Agency (ESA), ESAC, E-28692 Villanueva de la Canada, Madrid, Spain*

<sup>19</sup>*Purdue University, Department of Physics and Astronomy, 525 Northwestern Ave, West Lafayette, IN 4790720, USA*

<sup>20</sup>*Integrative Data Science Initiative, Purdue University, West Lafayette, IN 47907, USA*

<sup>21</sup>*Department of Astronomy, University of Virginia, Charlottesville, VA 22904-4325, USA*

<sup>22</sup>*Steward Observatory, University of Arizona, 933 N. Cherry St, Tucson, AZ 85721, USA*

<sup>23</sup>*Caltech/IPAC, Mailcode 100-22, Pasadena, CA 91125, USA*

<sup>24</sup>*Department of Physics, College of Physical Sciences and Technology, Hebei University, 071002 Baoding, China*

<sup>25</sup>*Key Laboratory of High-precision Computation and Application of Quantum Field Theory of Hebei Province, Hebei University, 071002 Baoding, China*

This paper has been typeset from a  $\text{\TeX}/\text{\LaTeX}$  file prepared by the author.